Supplementary Figures

A

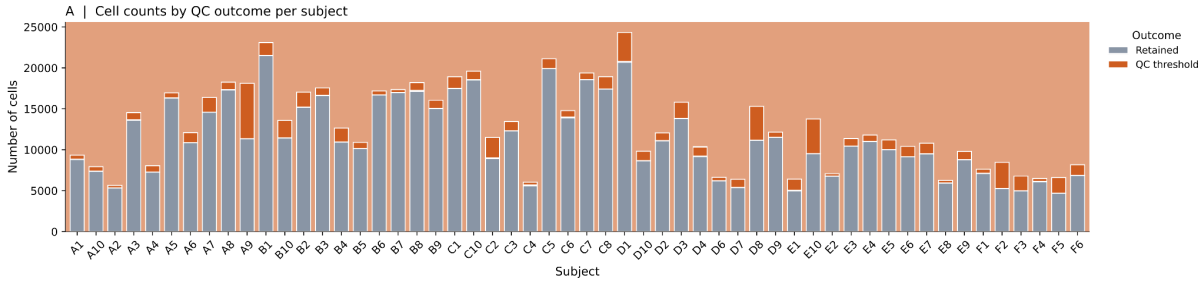

Supplementary Figure 1. Quality control cell filtering summary across subjects

A. Stacked bar chart showing the total number of nuclei per subject, coloured by QC outcome: retained nuclei (grey) and nuclei removed during quality control (red). Nuclei were excluded if they fell below 500 UMIs or 1,200 detected genes, exceeded 250,000 UMIs or 15,000 detected genes, had a mitochondrial transcript fraction above 10%, were flagged as doublets by Scrublet in more than 10% of 100 independent runs, or showed anomalous co-expression of marker genes from multiple cell lineages.

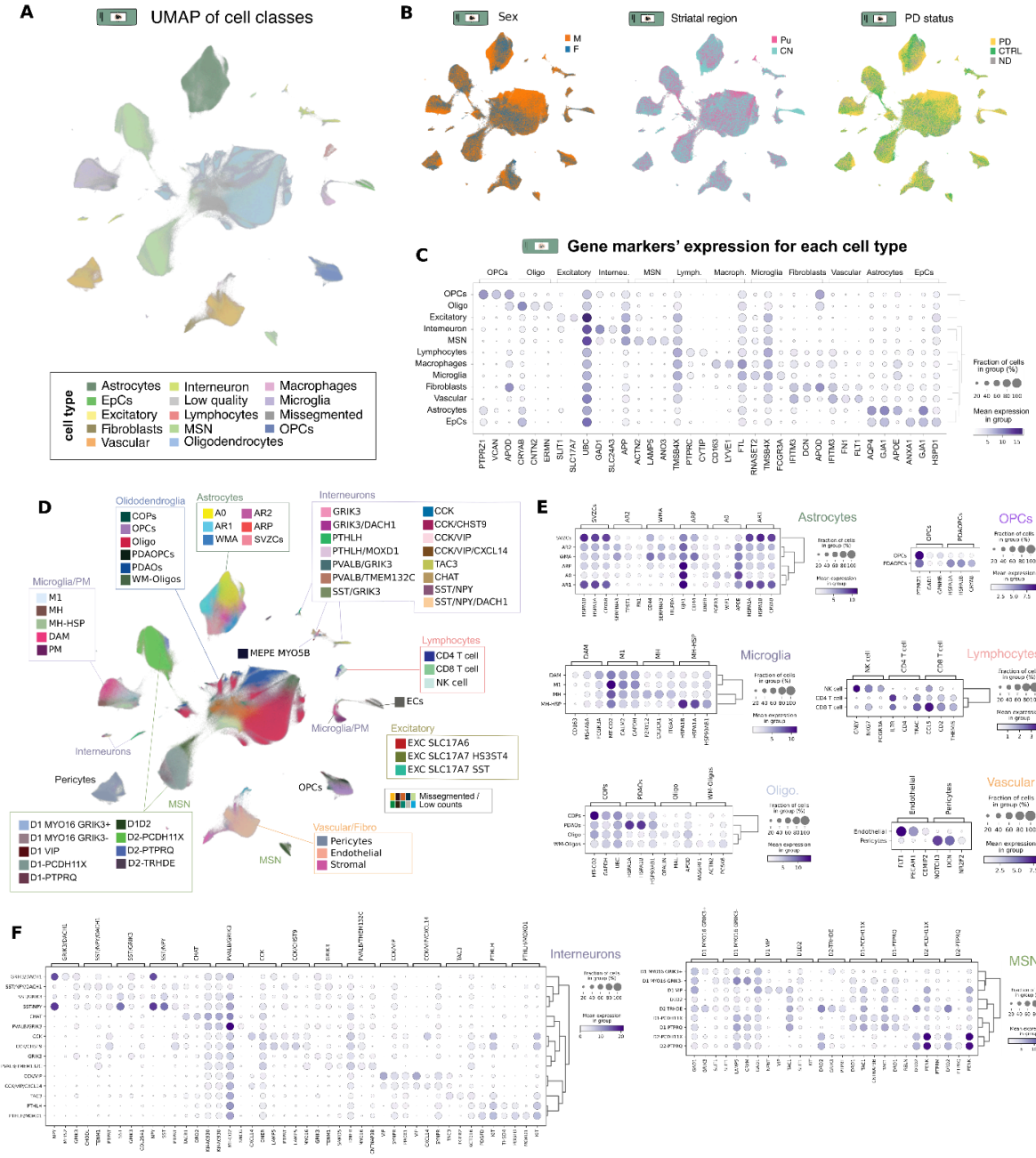

Supplementary Figure 2. Spatial transcriptomics characterization of cellular diversity

A. UMAP of cells profiled with Xenium, colored by cell type

B. UMAP of cells profiled with Xenium, colored by sex of donor (left), striatal region (middle) and PD status of the donor (left)

C. Dotplot illustrating the top 3 differentially expressed genes on each cell type identified in the Xenium dataset. Low quality and missegmented categories are left out of the visualization.

D. UMAP of cells profiled with Xenium, colored by subpopulation. Each cell type's legend including its subpopulations are presented as independent squares. Missegmented categories and Low counts are considered as one category.

E. Dotplot illustrating the top 3 differentially expressed genes of each subpopulation identified in Extended Data Figure 2D corresponding to non-neuronal subtypes.

F. Dotplot illustrating the top 3 differentially expressed genes of each subpopulation identified in Extended Data Figure 2D corresponding to Interneurons (left) and Medium spiny neurons (right).

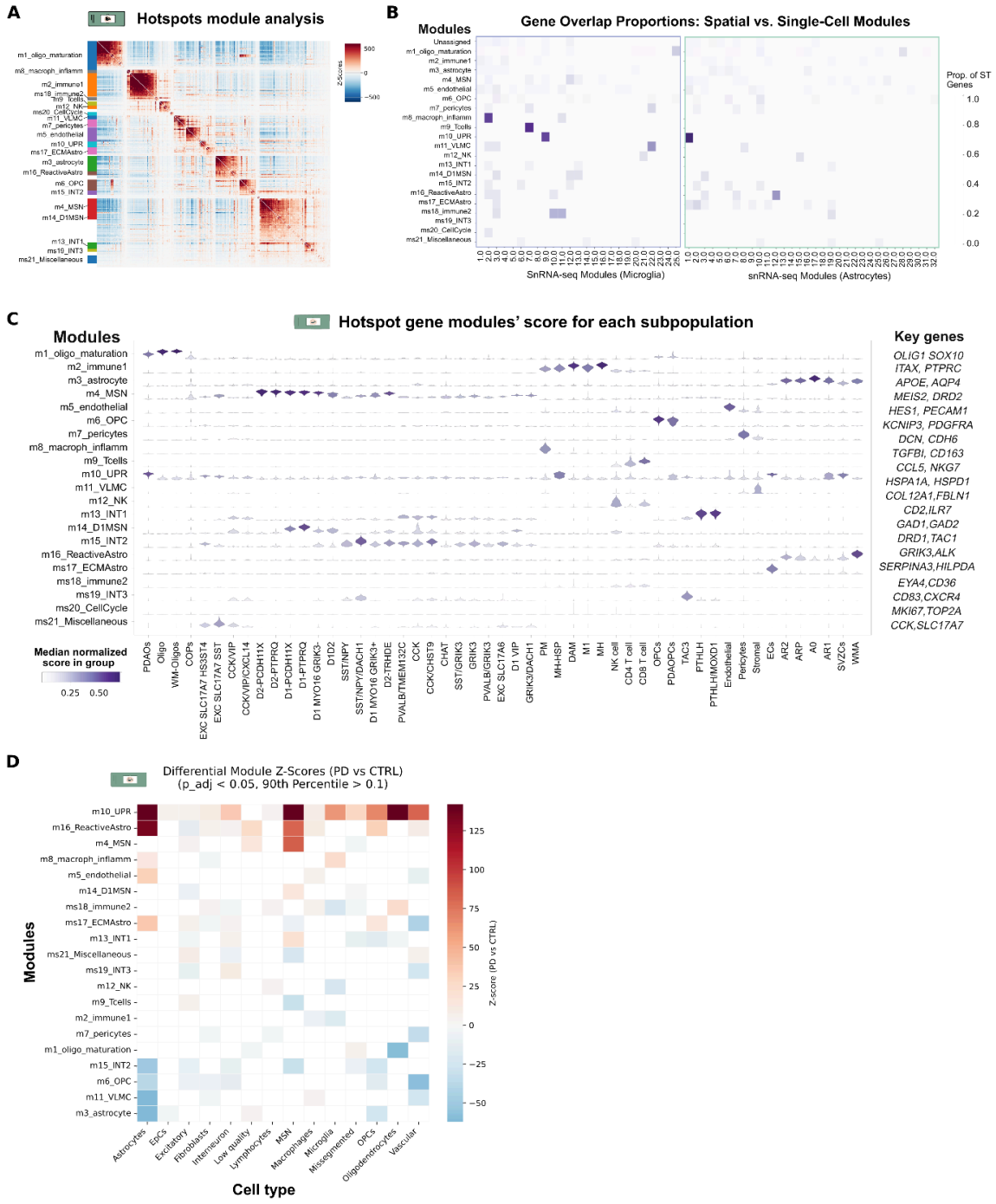

Supplementary Figure 3. Gene expression modules identified in Xenium datasets

A. Modules identified in the Xenium iST dataset using Hotspot, as represented by the z-score obtained from individual genes. Modules annotated are shown on the left bar.

B. Stacked violin plot representing the scores of cells within each subpopulation for each module identified using Hotspot in the Xenium iST dataset. Color of each violin indicate mean score in the subpopulation

C. Gene overlap between Xenium Hotspot modules and snRNA-seq modules (Astrocytes/Microglia). Color indicates the proportion of Xenium module genes identified within the snRNA-seq modules, accounting for Xenium's smaller panel size.

D. Heatmap of module score Z-scores (PD vs. Control) per cell type. Positive values indicate PD enrichment. Displayed values are restricted to differentially expressed modules (Wilcoxon $p<0.05$) where the 90th percentile module score within the cell type is >0; non-significant or low-expression modules are blank.

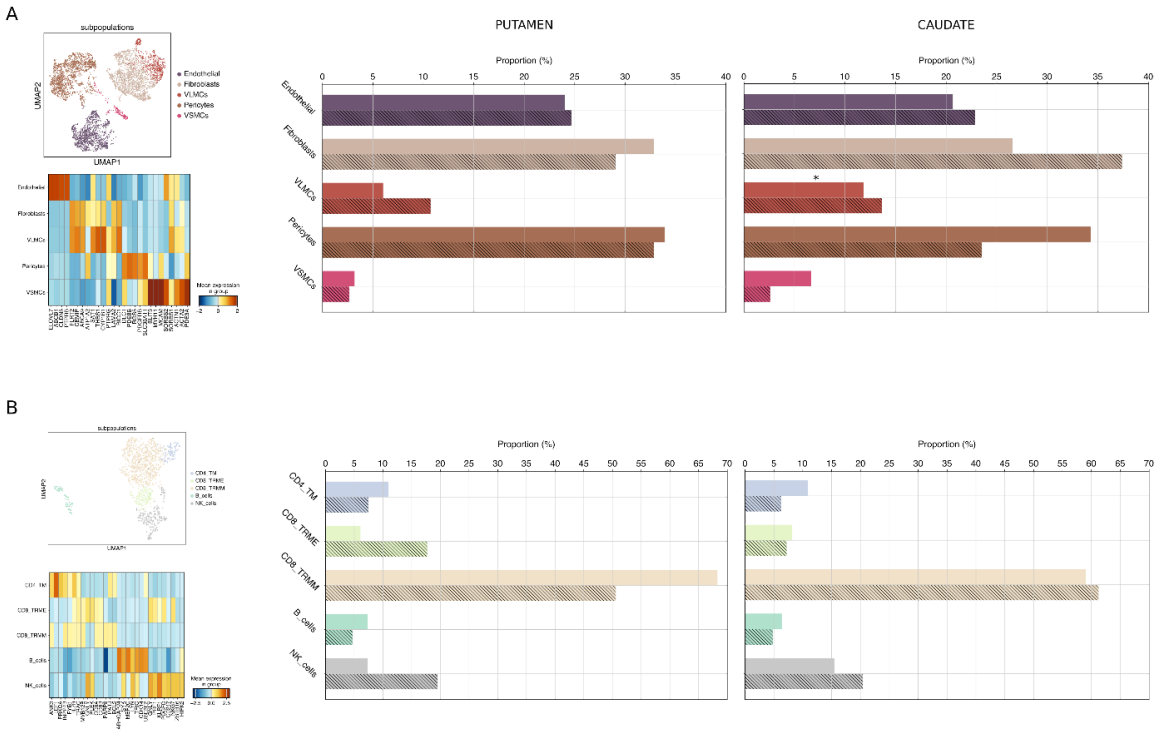

Supplementary Figure 4. Cellular heterogeneity and regional distribution of vascular-associated and lymphocyte subpopulations across conditions

A. UMAP representation of subpopulations associated with vascular niche (top) and their main markers represented with a heatmap showing the mean expression of each gene per group (bottom).

B. Barplots illustrating the frequencies of each subpopulation per Condition and Region

C. Top: UMAP embedding of lymphocyte subpopulations. Bottom: heatmap showing the key marker genes defining each subpopulation, with colormap representing the mean expression per subpopulation.

D. Relative abundance of each subpopulation across conditions and striatal regions

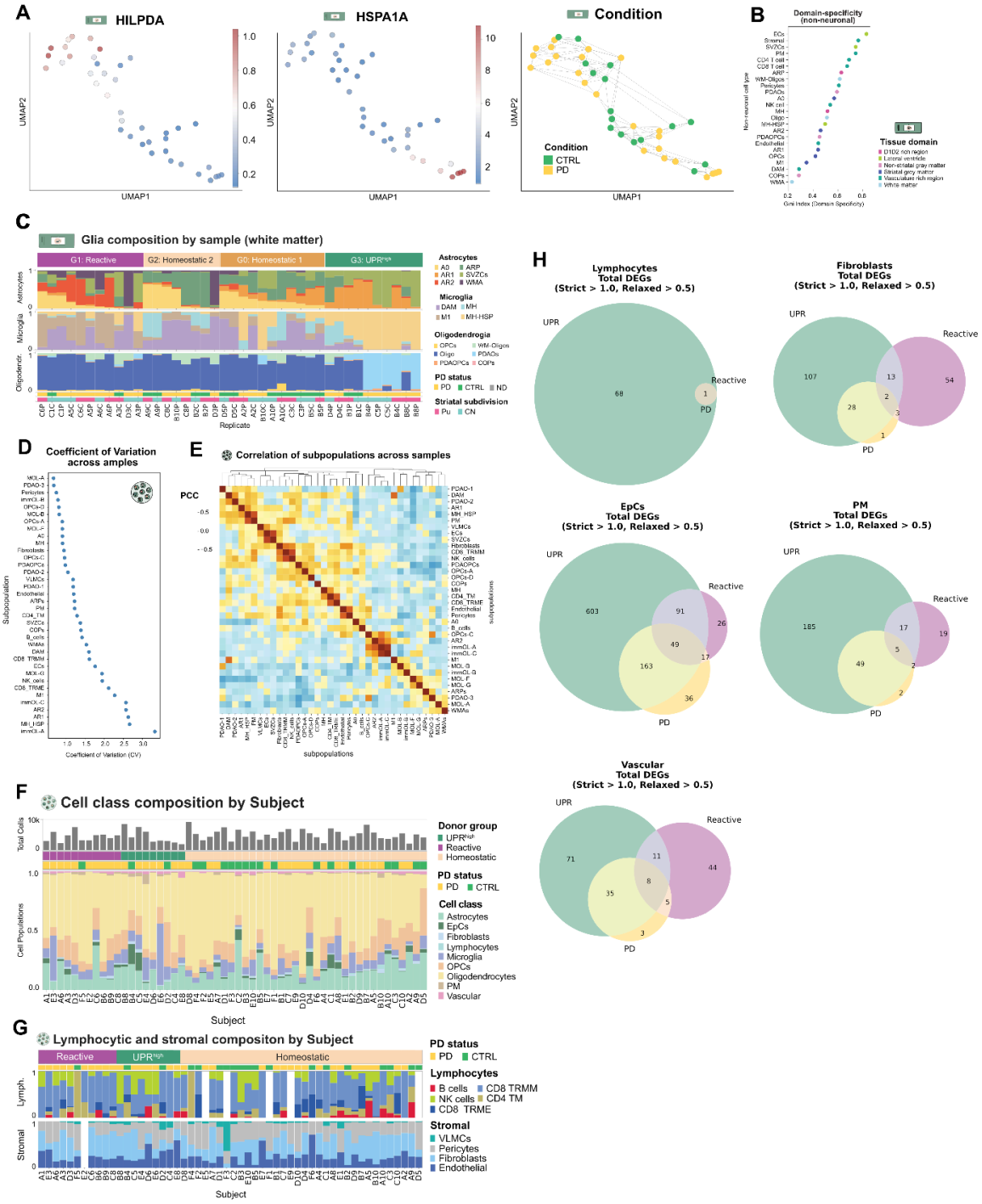

Supplementary Figure 5. Extended information regarding donor stratification

A. Spatial representation of Xenium datasets, in the form of a UMAP, with individual dots representing individual samples, considering only cells identified within the striatal gray matter domain. Samples are colored by PD status (right), HSPA1A (middle) and HILPDA (right) mean expression. .

B. Domain specificity of non-neuronal subpopulations. Dot plot showing the Gini inequality index (x-axis) for each subpopulation (y-axis). Higher Gini values indicate greater restriction to specific spatial domains. Points are colored by the domain of peak abundance.

C. Cell type-specific subtype composition in the white matter. The stacked bar plot illustrates the relative proportions of astrocyte, microglia, and oligodendroglia subtypes across Xenium samples. To provide context for each sample, the total cell count is indicated in the upper bar plot (top), while corresponding metadata, including PD status and donor group, are annotated directly above the compositional data.

D. Cell-type frequency variability across samples. Scatter plot showing the coefficient of variation (CV) for the relative abundance (x-axis) of each snRNA-seq subpopulation (y-axis) across all samples.

E. Correlation of cellular architecture across snRNA-seq samples. The heatmap illustrates the Pearson correlation of pairwise subpopulation abundances across all snRNA-seq samples.

F. Cell type-specific subtype composition in snRNA-seq. The stacked bar plot illustrates the relative proportions of cell types across snRNA-seq samples. To provide context for each sample, the total cell count is indicated in the upper bar plot (top), while corresponding metadata, including PD status and donor group, are annotated directly above the compositional data.

G. Transcriptional overlap across disease states. Venn diagrams depict shared and unique DEGs between PD, UPR-high, and Reactive groups for Lymphocytes (top,left), Fibroblasts (top, right), Ependymal cells (mid,left), perivascular macrophages (mid, right) and vascular cells (bottom)

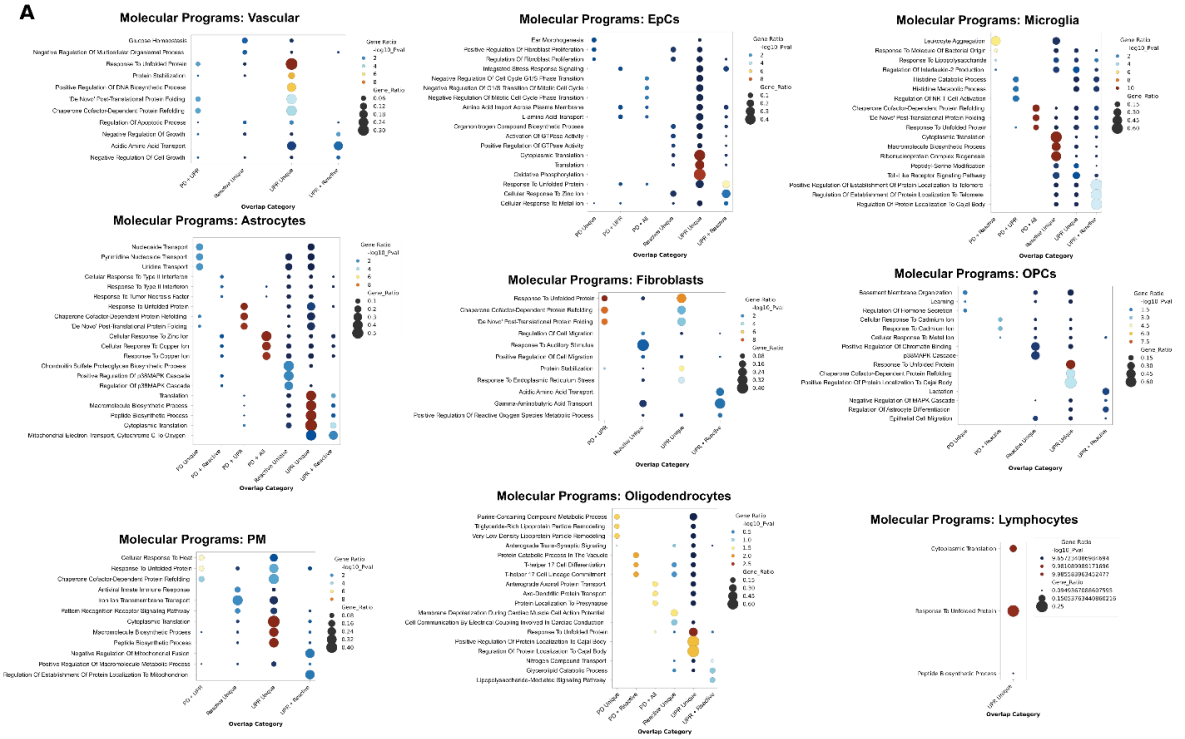

Supplementary Figure 6. GSEA exploration of genes differentially expressed intersecting between PD, Reactive and UPR-high donor groups

A. Enrichment of overlapping DEGs across PD, Reactive, and UPR-high donor groups. Dot plots show the top 3 enriched GO Biological Process (2023) terms for genes shared between these groups. Plots are stratified by cell type (facet), with gene subsets on the y-axis. Dot color represents −log10(p-value) and size represents the gene ratio. Only significantly enriched terms ($p<0.05$) are shown.

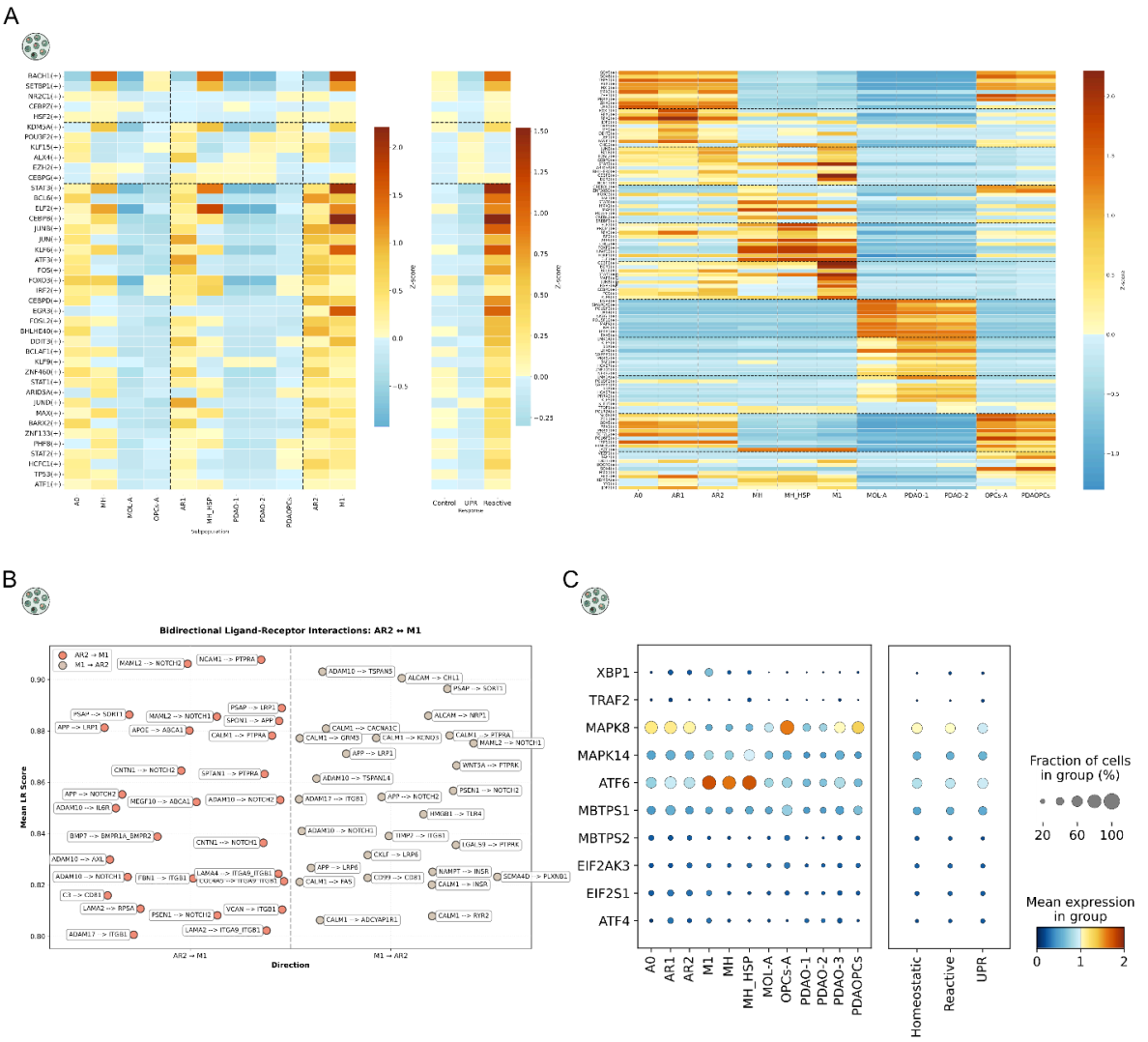

Supplementary Figure 7. Glial regulatory programs, intercellular communication, and unfolded protein response activity across disease-associated states

A. Matrixplot showing the activity of response-associated regulons across glial subpopulations, as inferred by the SCENIC workflow. Regulons shown were identified as significantly upregulated in subpopulations belonging to either the UPR or Reactive response category relative to control-like subpopulations, and were selected based on consistent enrichment across subpopulations sharing the same response program. Rows represent individual regulons; columns represent glial subpopulations grouped by response category (Control-like, UPR, and Reactive) (left). Matrixplot showing the activity of subpopulation-specific regulons across glial subpopulations. Regulons shown were identified as significantly upregulated in individual subpopulations, and were retained only if enrichment was not shared with other subpopulations (right).

B. Cell-cell interactions between AR2 astrocytes and M1 microglia as estimated by LIANA. Interactions where AR2 acts as the ligand-expressing cell and M1 as the receptor-expressing cell are shown in red; the reverse direction is shown in brown.

C. Dotplot showing the expression of canonical UPR pathway genes across glial subpopulations and molecular programs (Control-like, UPR, and Reactive). Genes are organized by UPR branch: IRE1α (XBP1, TRAF2, MAPK8, MAPK14), ATF6 (ATF6, MBTPS1, MBTPS2), and PERK arm (EIF2AK3, EIF2S1, ATF4). Dot size reflects the proportion of cells within each subpopulation expressing the gene; color intensity indicates mean expression level within the expressing fraction.

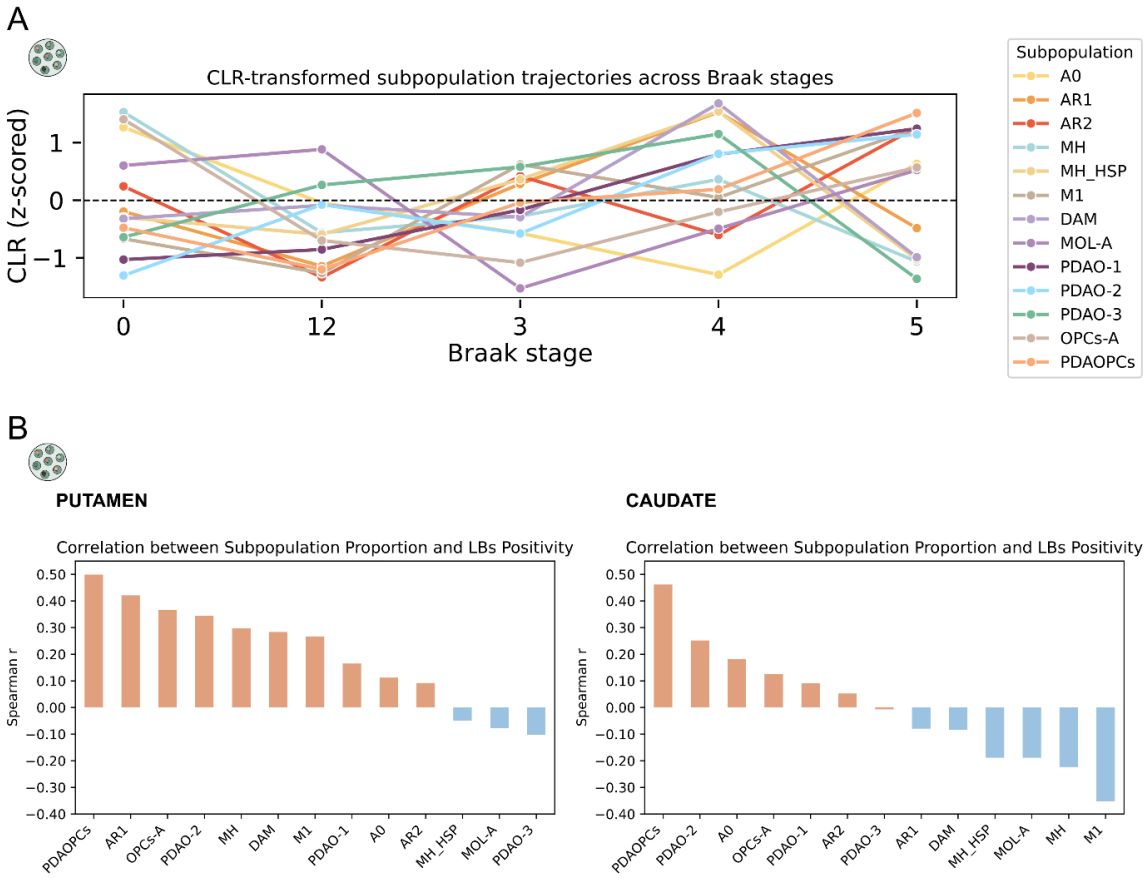

Supplementary Figure 8. Dynamics of glial subpopulation abundance across Braak stages and their association with Lewy body burden

A. Lineplot showing CLR-transformed abundance of each subpopulation across Braak stages.

B. Correlation analysis between subpopulations of interest and LB load both in Pu (left) and CN (right).